Duesterhoeft, E., Quinteros, J., Oberhänsli, R., Bousquet, R., de Capitani, C. (2014): Relative impact of mantle densification and eclogitization of slabs on subduction dynamics: A numerical thermodynamic/thermokinematic investigation of metamorphic density evolution. - *Tectonophysics*, *637*, pp. 20—29.

DOI: http://doi.org/10.1016/j.tecto.2014.09.009

Relative impact of mantle densification and eclogitization of slabs on subduction dynamics: a numerical thermodynamic/thermokinematic investigation of metamorphic density evolution

Erik Duesterhoeft[a,b,*], Javier Quinteros[c,d], Roland Oberhänsli[a], Romain Bousquet[a,b], Christian de Capitani[e]

[a] *Institute of Earth and Environmental Science, University of Potsdam, Karl-Liebknecht-Str. 24-25, 14476 Potsdam-Golm, Germany*
[b] *Institute of Geosciences, University of Kiel, Ludewig-Meyn-Str. 10, 24118 Kiel, Germany*
[c] *Deutsches GeoForschungsZentrum GFZ, Telegrafenberg, 14473 Potsdam, Germany*
[d] *Department of Computer Sciences, Facultad de Ciencias Exactas y Naturales, Universidad de Buenos Aires, Buenos Aires C1428EGA, Argentina*
[e] *Institute of Mineralogy and Petrography, University of Basel, Bernoullistrasse 30, 4056 Basel, Switzerland*

Abstract

Understanding the relationships between density and spatio-thermal variations at convergent plate boundaries is important for deciphering the present-day dynamics and evolution of subduction zones. In particular, the interaction between densification due to mineralogical phase transitions and slab pull forces is subject to ongoing investigations. We have developed a two-dimensional subduction zone model that is based on thermodynamic equilibrium assemblage calculations and includes the effects of melting processes on the density distribution in the lithosphere. Our model calculates the "metamorphic density" of rocks as a function of pressure, temperature, and chemical composition in a subduction zone down to 250 km. We have used this model to show how the hydration, dehydration, partial melting and fractionation processes of rocks all influence the metamorphic density and greatly depend on the temperature field within the subduction system. These processes are largely neglected by other approaches that reproduce the density distribution within this complex tectonic setting. Our model demonstrates that the initiation of eclogitization (i.e., when crustal rocks reach higher densities than the ambient mantle) of the slab is not the only significant process that makes the descending slab denser and generates the slab pull force. Instead, the densification of the lithospheric mantle of the sinking slab starts earlier than eclogitization and contributes significantly to slab pull in the early stages of subduction. Accordingly, the complex metamorphic structure of the slab and the mantle wedge has an important impact on the development of subduction zones.

Keywords: density, melt, metamorphism, subduction, thermodynamic modeling, thermo-mechanical modeling

1. Introduction

Subduction zones, regions where two tectonic plates converge and the denser plate sinks beneath the other, are distributed worldwide and, along with seafloor spreading, represent the core process of plate tectonics (e.g., Isacks et al., 1968; Le Pichon, 1968; Morgan, 1968). These regions are characterized by strong earthquakes and volcanic eruptions, which significantly affect human life and destroy habitats. Therefore, it is crucial to further understand this geological process. However, the limited observations at depth and differing timescales complicate investigations. Numerical simulations in combination with observed geological and measured geophysical data can make up for the lack of observations (Gerya, 2011, and references therein). Many discussions concern the mechanisms that drive this complex tectonic system and the influence of volatiles, phase transitions, melt generation and the chemical composition of the descending and overriding slabs (Billen, 2008; Grove et al., 2012; Quinteros and Sobolev, 2012; Stern, 2002). It is assumed that in the majority of cases the primary force driving plate movement is the excess density of the descending slab's lithosphere (Davies, 1999; Forsyth and Uyeda, 1975; Vlaar and Wortel, 1976) due to the cooling of the plate surface as the oceanic plate moves away from the spreading ridge (Oxburgh and Parmentier, 1977). Consequently, the density distribution in the lithospheric slab and the change of density due to the change of pressure and temperature (P-T) conditions in subduction zones play a significant role in understanding plate dynamics. The

*Corresponding author.
Email address: ed@min.uni-kiel.de (Erik Duesterhoeft)

Table 1: A summary of model parameters.

parameter	value
slab dip (°)	35
slab age (Ma)	41
subduction velocity (cm/a)	7.7
basal temperature of lithosphere (°C)	1450
depth of the base of the model (km)	670
total model length (km)	1000
total time of evolution (Ma)	11
MORB layer thickness (km)	7.0
bulk rock composition after	Hofmann, 1988
Serpentinite layer thickness (km)	2.0
bulk rock composition after	Li et al., 2004
Harzburgite layer thickness (km)	21.0
bulk rock composition after	Ganguly et al., 2009
Lherzolite layer thickness (km)	65.0
bulk rock composition after	Brown and Mussett, 1993

density behavior of subducting and overriding plates have been studied using several approaches, such as the following: a) gravimetrical measurements (e.g., Prezzi et al., 2009; Tašárová, 2007); b) seismics/tomography (e.g., Kárason and Van der Hilst, 2002; Zhao, 2001); c) petrologic investigations (e.g., Connolly and Kerrick, 2002; Hacker et al., 2003; Sobolev and Babeyko, 1994; Ringwood and Green, 1966); and d) numerical simulations (e.g., Doin and Henry, 2001; Gerya et al., 2004; Sobolev et al., 2006; van Keken et al., 2008).

In this study, our focus is on the density evolution of subducting slabs. McKenzie (1969) first noticed the importance of mineralogical changes on the negative buoyancy force of a sinking slab during subduction, demonstrating the effect of metamorphic densification at the transformation of oceanic crust (basalt and gabbro) to eclogite. This so-called "metamorphic density" is a function of temperature, pressure and chemical composition and has a large influence on lithospheric dynamics (e.g., Duesterhoeft et al., 2012; Goffé et al., 2003; Henry et al., 1997). Modeling the density structure of the lithosphere solely by fixed physical parameters (thermal expansivity and bulk modulus) based on the fixed chemical composition of each layer is not adequate because the mineral reactions within each layer significantly influence the rock density (e.g., Afonso et al., 2005; Bousquet et al., 1997, 2005; Duesterhoeft et al., 2012; Le Pichon et al., 1997). Most thermodynamic studies of subduction zones focus on the density structure of the upper part of the mantle (≈ 200-660 km depth). Below 200 km, the basaltic layer of a descending slab is always heavier than the lower harzburgitic layer (Ganguly et al., 2009). Bina et al. (2001) showed how phase changes in the transition zone at depths of 410-660 km are perturbed by the thermal environment and result in density anomalies that may affect the subduction rate. Similarly, the subduction rate influences the thermal structure and thus the density structure of a subduction zone because it depends on the convergence rate of the descending and overriding plates. Here, we study the upper 250 km of the lithosphere of a young (41 Ma), shallow (35 °), fast (77 km/Ma) and thus cold subduction zone (yielding a slab thermal parameter Φ = slab age * vertical descent rate = 1800 km). By analyzing the density and metamorphic structure of such a subduction zone, we may gain knowledge about the major, and thus driving, metamorphic processes in the upper 250 km of the subduction zone. These processes are the breakdown of hydrous minerals and the release of fluids or the generation of partial melts. Moreover, investigating the metamorphic density structure in a 2D thermodynamic approach may provide new insights into the initiation of subduction and the exhumation process of low-temperature, high-pressure metamorphic rocks (e.g., blueschist and eclogite) that characterizes paleosubduction zones (e.g., Giunchi and Ricard, 1999; Guillot et al., 2009; Pourteau et al., 2010).

2. Methods

The modeling of subduction is performed by means of two different and independent approaches. In the first, a simple 2D model with a kinematically prescribed slab and a constant subduction rate (Table 1) is used. The advantage of a simple model is the limited parameter space, which allows the investigation of the "metamorphic density" in a systematic manner (Gerya, 2011). Therefore, we calculate the thermal structure down to a depth of 670 km (with a vertical resolution of 1000 m) to generate a steady state subduction zone. In the second approach, we use a thermo-mechanical model in which the subduction rate is prescribed, but the evolution of the slab is self-consistent. This

means that only the subducting velocity is imposed, but the variations in the subduction angle, bending, unbending and other related processes are coherent with the state of the system as a whole. In the calculation of the metamorphic density structure of subduction zones, the study focuses only on the upper part (0-250 km depth) because it is the part in which most mineralogical changes take place. Furthermore, it is the region of greatest seismic activity.

2.1. Temperature-pressure setting

We use the kinematic finite-difference heat transfer algorithm TEMSPOL (Negredo et al., 2004), an open MATLAB® code, to calculate temperature distributions in subduction zones. The thermo-kinematic model is calculated by solving the 2D heat equation, including adiabatic heating, radioactive heat generation, latent heat and frictional heating (the last two are not taken into account in our calculations). Here, the surface temperature is taken as 0 °C and the temperature at the base of the lithosphere is 1450 °C (Jaupart and Mareschal, 2011; Stein and Stein, 1992). We modified the code to model the thermal structure of more than two layers (the oceanic crust and the mantle). The modification subdivides the 95-km-thick oceanic slab, from top to bottom, into a MORB layer (7 km thick), a serpentinite layer (2 km thick), a dry harzburgite layer (21 km thick) and a dry lherzolite layer (65 km thick). These subdivisions are implemented to evaluate the different effects of the chemical bulk composition of each layer on the slab's mineralogical changes (Ganguly et al., 2009; Ringwood and Irifune, 1988). Calculating the metamorphic density also requires the corresponding pressure of each temperature in our model, which is computed lithostatically from the thermo-kinematic model. We know that this is a valid first-order approximation, and we keep in mind that there could be certain additional tectonic over- and underpressure effects (Babeyko and Sobolev, 2008; Li et al., 2010; Petrini and Podladchikov, 2000). We checked the influence of these effects on our results by using full dynamic pressure from a thermo-mechanical model (see supplementary material).

A second set of pressure and temperature distributions was calculated by means of a thermo-mechanical model (see supplementary material). We use an enhanced 2D version of SLIM-3D, a code (Popov and Sobolev, 2008; Quinteros and Sobolev, 2013) suitable for simulating the evolution of a subducting slab in a self-consistent manner (gravity driven) in a vertical cross-section through the upper mantle. The model has a true free surface, includes elastic deformation and utilizes nonlinear temperature- and stress-dependent visco-elasto-plastic rheology. The domain is 1400 km wide and 670 km deep. On the left side, the overriding plate is moved eastwards throughout the whole simulation with a velocity of 3 cm/a, while the subducting plate is pushed at 4.7 cm/a (resulting in a total subduction velocity of 7.7 cm/a). On the left side of the model, a lithostatic pressure boundary condition is applied under the overriding plate. This leaves the major part of the side open, allowing the material to enter and exit the model in a realistic way. A subduction channel is considered to be a well-lubricated interface with weak ductile rheology and a low friction coefficient, which favors the development of realistic one-sided subduction (Gerya et al., 2008; Sobolev and Babeyko, 2005).

2.2. Thermodynamic modeling

The metamorphic density is determined by accounting for the mineralogical changes that occur with changes in temperature and/or pressure. Therefore, we apply the Theriak/Domino software (version 01.08.2009; de Capitani and Petrakakis, 2010) to calculate the metamorphic density using the principle of minimized ("apparent") Gibbs free energy, $\Delta_a G$ (de Capitani and Brown, 1987). We use an updated thermodynamic database from Berman (1988), called JUN92.bs (de Capitani and Petrakakis, 2010), for crustal rocks and the updated thermodynamic database from Holland and Powell (1998), called tcdb55 (de Capitani and Petrakakis, 2010), for the harzburgite and lherzolite layers. Because each database has its own strengths and weaknesses, the use of two different databases is necessary to obtain better accuracy in the modeling. The tcdb55 database offers an approach to modeling the effects of melt production and hydrated HP phases in ultramafic rocks but is based on an invalid Landau free energy term, ΔG_{Land}, published by Holland and Powell (1998). This term significantly affects the volume calculation (and thus the density calculation) of certain mineral phases, e.g., alpha-quartz and feldspar (e.g., Duesterhoeft, 2013), leading to a false standard volume. For example, the alpha-quartz volume under room conditions clearly appears to be too high (V_0=22.8945 cm^3/mol) compared with experiments (V_0 =22.69 cm^3/mol; Raz et al., 2002; Robie and Hemingway, 1995). Generally, we assume that the JUN92.bs represents the rock density better on a lithospheric scale. However, we use the tcdb55-database to model the harzburgitic (composition after Ganguly et al., 2009) and lherzolitic layers (composition after Brown and Mussett, 1993), because JUN92.bs lacks thermodynamic melt models.

Unfortunately, the melt model of the tcdb55 database is adjusted to an andesitic melt. The melt model fails for our ultramafic bulk rock compositions, resulting in unrealistic melt generation below 600 °C. Therefore, we have to modify the thermodynamic data for the water component "LIQtc_h2O" in the tcdb55 database ("h2oL" in Holland and Powell, 1998). We fit the volume of dissolved H_2O in silicate liquids to the predictions of Ghiorso et al. (2002)

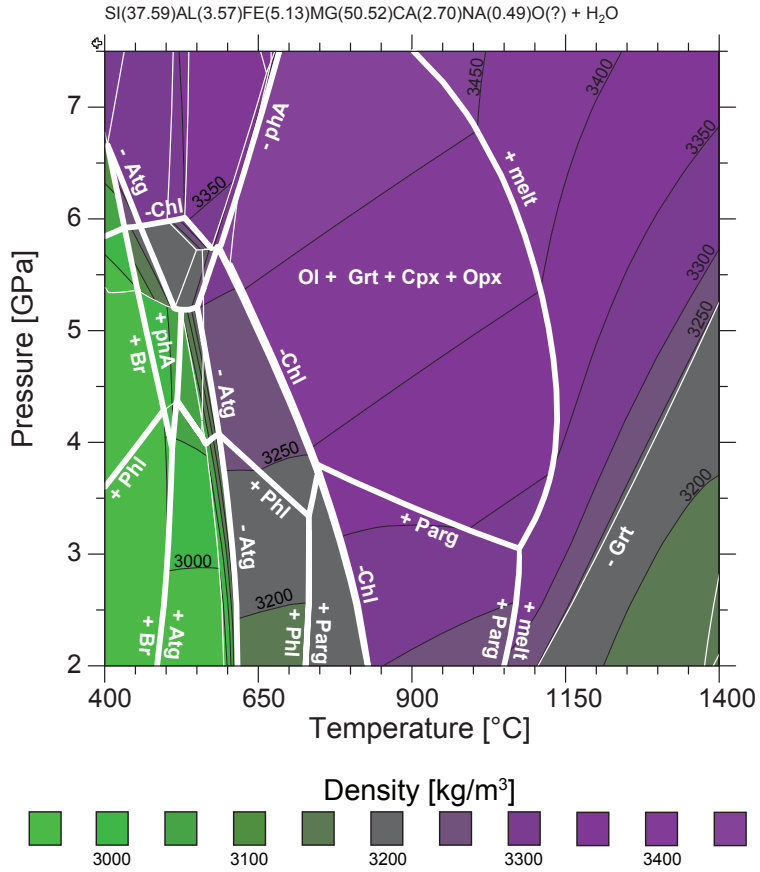

Figure 1: Density isoline plot calculated for a fully hydrated lherzolitic composition from Brown and Mussett (1993) using Domino software (de Capitani and Petrakakis, 2010) and an improved H_2O-melt component (see 2.2). Note the density increase at the reactions (white lines), in which antigorite and chlorite break down. Mineral abbreviations: Atg - antigorite, Br - brucite, Chl - chlorite, Cpx - clinopyroxene, Grt - garnet, melt - partial melt, Ol - olivine, Opx - orthopyroxene, Parg - pargasite, phA - phase A, Phl - Na-phlogopite.

and calculate the enthalpy and entropy for the reaction "Forsterite + H_2O = Liquid" of Ellis and Wyllie (1979). In addition, we have to update the Margules parameter (see supplementary material). Subsequently, the values fit the phase relations among the other melt components, and the new H_2O component features the same position in a binary diagram as before (using the tcdb55 database). The new "LIQtc_h2o" melt species results in more realistic densities and melt stability fields (Fig. 1). However, the fayalite melt species is problematic for pressures above 4 GPa, bending the solidus line of a water-saturated ultramafic rock to lower temperatures than those observed in experiments (see Fig. 5 in Grove et al., 2012). This difference is because experiments on fayalite melting are absent. Nonetheless, using the newly modified "LIQtc_h2o" data more closely reproduces experimental data for a water-saturated lherzolite.

2.3. Water transfer and metamorphic density

In subduction zones, three major slab lithologies allow the transport of water to a greater mantle depth: a) hydrated sediments, b) basaltic oceanic crust and c) serpentinized mantle. Rüpke et al. (2002) compared the three lithologies and inferred that a serpentinized mantle is the best medium to carry chemically bound water because it can store significant amounts of water in the form of hydrous mineral phases (i.e., minerals that contain hydrogen in their chemical structure; mostly hydroxyl (OH^-) groups or crystal water). Serpentinized mantle is stable to a much greater depth than the hydrous minerals of oceanic crust or sediments (Ulmer and Trommsdorff, 1995). Additionally, Hacker (2008) argued that the flux of H_2O to great depth in cold slabs is dominated by the basaltic oceanic crust and serpentinized mantle and is proportional to the bulk rock H_2O content. Stern (2002) suggested that the oceanic crust is composed of a small amount of serpentinite, which is important for the transport and release of water during subduction (Lee and Chen, 2007). Therefore, we subdivide the oceanic crust into a water-saturated 7-km-thick MORB layer (composition after Hofmann, 1988) and a water-saturated 2-km-thick serpentinite layer (composition after Li et al., 2004; Bucher and Grapes, 2011) at its base. We neglect the effect of sediments for the following reasons: 1) sediments do not trans-

port a large amount of water to a greater depth (> 50 km; Rüpke et al., 2002); 2) a model resolution of 1 km would cover the thickness of a sediment layer; 3) applying thermodynamic databases to sedimentary bulk rock compositions is insufficient (e.g., they ignore pore space and biotic material); and 4) the chemical bulk compositions of sediments vary widely (e.g., supplemental material of Poli and Schmidt, 2002).

In our model, each cell has a value for temperature, pressure, chemical bulk composition and the applied thermodynamic database. To model the chemical water transfer and metamorphic density, we use THERIAK_D, an add-on for the Theriak/Domino software (Duesterhoeft and de Capitani, 2013). THERIAK_D transferred the input parameters (temperature, pressure, chemical composition of the rock and thermodynamic database) from MATLAB® to Theriak to first calculate the number of moles of released free water and the solid bulk rock density (i.e., without the density of the free fluid). Thus, the amount of free water and metamorphic solid bulk rock density are computed "in situ" (i.e., not using pre-computed look-up tables) in our model. In MATLAB®, the released amount of free hydrogen is added to the chemical bulk rock composition of the cell above. In this way, we generate a vertical water transfer (e.g., Arcay et al., 2005; Hebert et al., 2009b; Wada et al., 2012). The absorption or release of fluids depends only on thermodynamically predicted stable mineral assemblages. If a hydrous mineral phase becomes stable in an equilibrium mineral assemblage, it will absorb available free water (i.e., hydrogen is incorporated into the crystal structure) as long as the assemblage is not saturated in water (i.e., each possible hydrous mineral phase is already stable). In contrast, if a hydrous mineral phase participates in a dehydration reaction and no longer stable, the excess water will be released (i.e., excess hydrogen is passed upward to the next cell). As a consequence, the excess unabsorbed and released water migrates progressively upwards cell-by-cell until being absorbed by a newly formed hydrous mineral phase (Peacock, 1987) or until it reaches the earth surface (upper model boundary). We assume that metamorphic hydration and dehydration reactions are geologically short-lived processes, so we neglect their kinetics. In this context, John et al. (2012) suggest that fluid migration rates are extremely high and that slab dehydration results in short-lived, pulsed, channelized fluid-flow events along fracture systems (with a duration of only ~200 years). The assumption of rapid metamorphic hydration/dehydration processes is consistent with the one of John et al. (2012). Of course, this approach may not be realistic, but estimating the real reaction rates as a function of largely unknown dimensions, timescales and reaction kinetics is highly challenging (Arcay et al., 2005; Peacock, 1996).

3. Results

Our model calculates the metamorphic density, based on thermodynamic modeling, in relation to the corresponding pressure and temperature conditions in a subduction zone. In a second step, the migration of free water is computed based on fixed steady state *P-T* field and equilibrium calculations. When melting occurs, we consider only the solid rock density. To model the chemical composition of the solid rocks, and hence the density, we used two different approaches: a) without and b) with melt segregation, i.e., the produced partial melt is separated and removed from the residual lithospheric bulk rock composition. As a result, the solid rock density predictions differ and are discussed below. In the second approach, partial melt is always removed completely from the system after formation and, thus, does not interact with the surrounding lithospheric mantle.

3.1. Steady-state density calculations

Our first calculation is based on the pressure and temperature results from TEMPSOL and represents the thermal steady state after 11 Ma (Fig. 2). The calculated metamorphic densities denote the densities of equilibrated mineral assemblages. The water release should be viewed as the first release of water at the current time because the mantle wedge is assumed to be dry initially. This assumption aims to simplify the representation of the initiation of mantle wedge hydration. At an approximate depth of 60 km, a significant density change in the dry lithospheric mantle is caused by the well-known transition of spinel to garnet. Gradual density changes in the lithospheric mantle are caused by the changes of thermal expansion and the compressibility of the minerals, and these changes are influenced by temperature, pressure and the molar ratios among olivine, pyroxene and garnet. The MORB layer of the descending slab exhibits more and greater density changes due to phase transitions. Up to 4 GPa, only minor density changes occur in the oceanic crust. In the modeled cold slab, the titanium silicate sphene breaks down at approximately 100 km (or 3 GPa) and is replaced by the high-pressure phase rutile via a divariant reaction, accompanied by modal increase in clinopyroxene at the expense of less-dense glaucophane and chlorite. This results in a density change of 20 kg/m^3 (from 3240 kg/m^3 to 3260 kg/m^3). The next minor density increase (20 kg/m^3) is caused by the breakdown of the sodium amphibole glaucophane at approximately 3.4 GPa in our model. The first significant density change (100 kg/m^3) occurs with the breakdown of chlorite between 4 and 5 GPa (Schmidt and Poli, 1998), followed by another important change (>100 kg/m^3) due to the occurrence of garnet (3600 kg/m^3) during eclogitization. All these

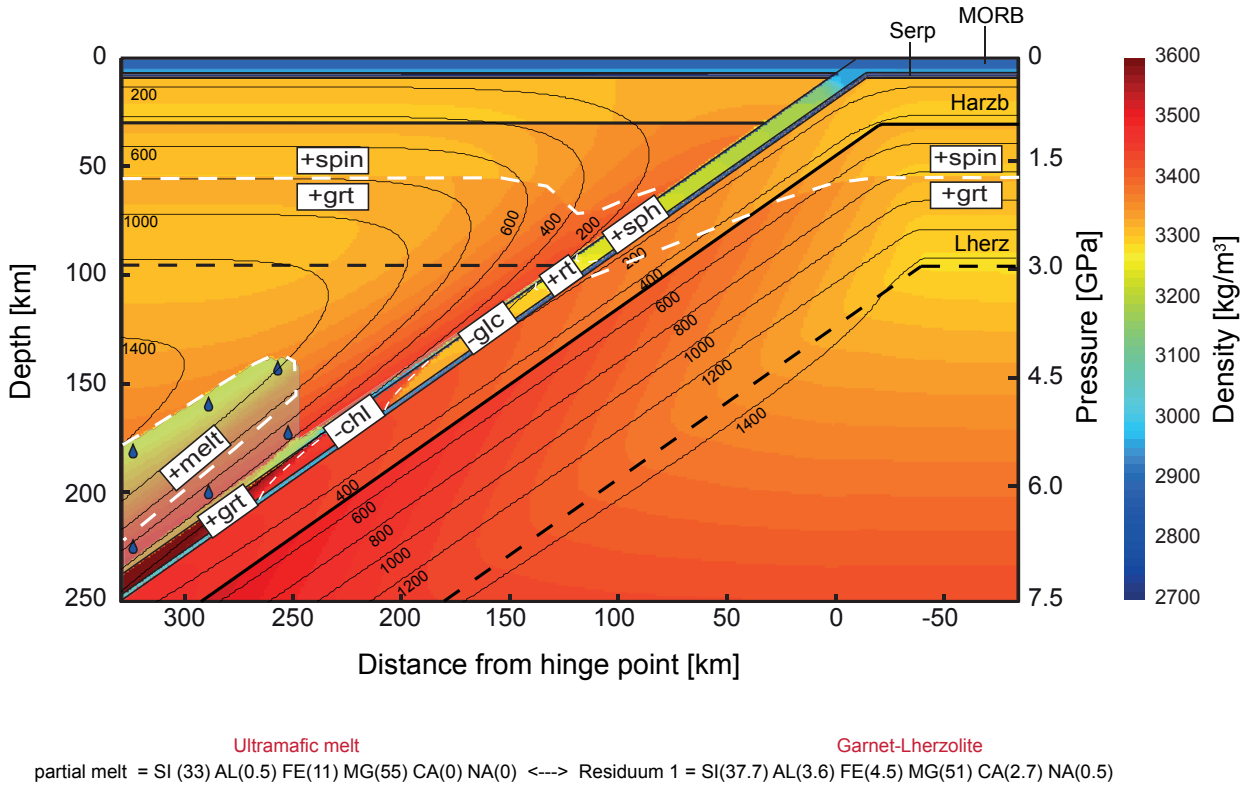

Figure 2: A 2D steady-state metamorphic density model of a subduction zone. Eclogitization starts where garnet (3600 kg/m^3) becomes stable in the MORB layer. Partial melting (assuming no melt segregation and fractionation processes) occurs as long as free water (shaded area with blue drops) is present and results in a slightly less dense mantle above the slab-wedge interface (see 3.1). Isotherms are given in Celsius degrees. Dashed black line - base of the lithosphere. Dashed white lines - stability limits of certain phases (white boxes). Abbreviations: chl - chlorite, glc - glaucophane, grt - garnet, Harzb – harzburgite layer, Lherz – lherzolite layer, melt - partial melt, rt - rutile, Serp – serpentinite layer, sph – sphene, spin – spinel.

breakdown reactions are mainly temperature sensitive and variations in the *P-T* field result in different phase transition depths.

In cold subduction zones, the temperature is low at the slab-mantle wedge interface of the downgoing slab. Therefore, super-hydrous mineral phases (serpentines) are stable in the mantle wedge. These minerals act like a sponge during their formation, absorbing all the water in a hitherto dry mantle wedge (e.g., Guillot et al., 2009) and might form a low-viscosity channel (e.g., Gerya et al., 2002; Hebert et al., 2009a). Above 6 GPa and 500 °C, the dry mantle wedge is no longer able to store a large amount of water. As a result, free fluids (calculated as water) can migrate upward (Fig. 2). Due to the migration, water acts as a catalyst for phase transitions and melt production (e.g., Wayte et al., 1989). Hence, the lherzolitic mantle partially melts at approximately 1000 °C. This first wet melt has an ultramafic composition and comprises the chemical elements magnesium, iron, silicon and hydrogen with a (Mg+Fe)/Si molar ratio of 2.0. Kawamoto and Holloway (1997) showed that an ultramafic melt is not uncommon in the case of a fully hydrated mantle at high pressure. Their experimental partial melts uniformly became more mafic with increasing pressure from an andesitic composition at 1 GPa to more mafic than the starting peridotite at 10 GPa. They showed that partial melting of H_2O-saturated peridotites at pressures greater than 5 GPa produced ultramafic melts with a (Mg+Fe)/Si molar ratio of 1 (pyroxene) at 5 GPa and 2 (olivine) at 10 GPa. Consequently, the residual lherzolitic mantle loses these elements (Mg and Fe) and becomes lighter because the residual is depleted in the heavy element iron. In our model, the mantle stops melting when all free water, which was released by the slab, is absorbed by the partial melt (Fig. 2). Note that the density of the residual mantle strongly depends on the thermodynamic database. As mentioned above (see 2.2), the thermodynamic fayalite component of the melt, which is responsible for the iron content of the melt, may overestimate the absorption of iron into the melt above 4 GPa. Therefore, the residual mantle could be too light, based on insufficient experimental data to extract good thermodynamic data for high-pressure rocks.

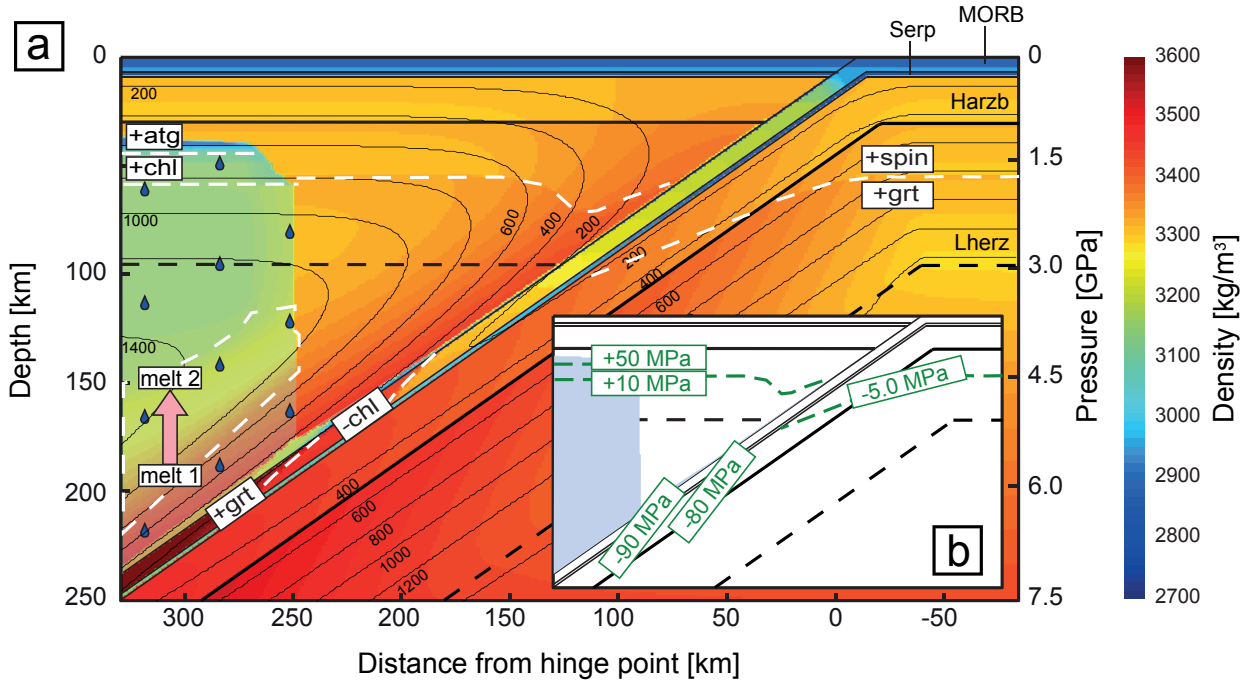

Ultramafic melt — Garnet-Lherzolite

partial melt 1 = SI (33) AL(0.5) FE(11) MG(55) CA(0) NA(0) <---> Residuum 1 = SI(37.7) AL(3.6) FE(4.5) MG(51) CA(2.7) NA(0.5)

Aluminum-rich melt — "Harzburgite"

partial melt 2 = SI (38) AL(22.5) FE(0.6) MG(27.5) CA(10.8) NA(0.6) <---> Residuum 2 = SI(38.4) AL(0.4) FE(0.02) MG(59.13) CA(2) NA(0.05)

Figure 3: a) 2D steady-state metamorphic density model of a subduction zone, assuming melt segregation. As a consequence, partial melts become more aluminum-rich, leaving a "harzburgitic" residual mantle. In addition, less water can be stored in the mantle than in Fig. 2, resulting in a further rise of free water until hydrous mineral phases (amphibole, chlorite, and serpentine) become stable. b) Hydration and dehydration processes result in overpressure (+) resp. underpressure (-) of up to 100 MPa in comparison with the surrounding area (green boxes). Isotherms are given in Celsius degrees. Dashed black line - base of the lithosphere. Dashed white lines - stability limits of certain phases (white boxes). Abbreviations: atg – antigorite, chl - chlorite, grt - garnet, Harzb – harzburgite layer, Lherz – lherzolite layer, melt 1- partial melt 1, melt 2- partial melt 2, Serp – serpentinite layer, spin – spinel.

3.2. The effect of melt segregation

To model the effect of melt segregation (Fig. 3), the composition of the partial melt is subtracted from the previous mantle bulk composition in a column and is normalized again during density calculation. Thus, the effect of mantle depletion is carried along each column from bottom to top, whereby the residual composition of a cell becomes the starting composition for the next cell. The upward transfer of the last fractionated residual composition, even if melt is no longer produced, displays mantle fractionation through time (see Fig. 4). In Fig. 3, the density distribution in the descending slab remains the same as in the scenario without melt segregation, whereas the density in the mantle wedge is different from the previous scenario. Due to melt segregation, the composition of the residual mantle changes from lherzolitic to harzburgitic. Consequently, the molar ratios of minerals and therefore the position of phase transitions in *P-T* space changes. As a result, less hydrogen can be stored in the melt (which is removed from the system in our calculation) and a free water fluid can migrate farther upward, similar to the previous calculation (see Fig. 2). Free water is absorbed only after the stabilization of hydrous mineral phases in the residual harzburgitic mantle below 800 °C (Fig. 3). A hydrated lithospheric mantle is significantly less dense than a dry mantle (up to 500 kg/m^3). Figure 3 shows that the residual mantle is also less dense (> 100 kg/m^3) than the original dry lherzolitic mantle. Simon and Podladchikov (2008) showed that such a density reduction is caused by the decrease of Al_2O_3. However, the fayalite melt component in the thermodynamic database (as discussed before) may underestimate the density of 3200 kg/m^3 of the fractionated mantle wedge (Fig. 3).

Within the mantle wedge, the composition of the extracted partial melt, an ultramafic wet melt, changes with increasing temperature. The partial melt becomes enriched in aluminum (Fig. 3) with the breakdown of garnet to orthopyroxene (Fig. 1). Consequently, the partial melt can absorb other incompatible elements, such as calcium and

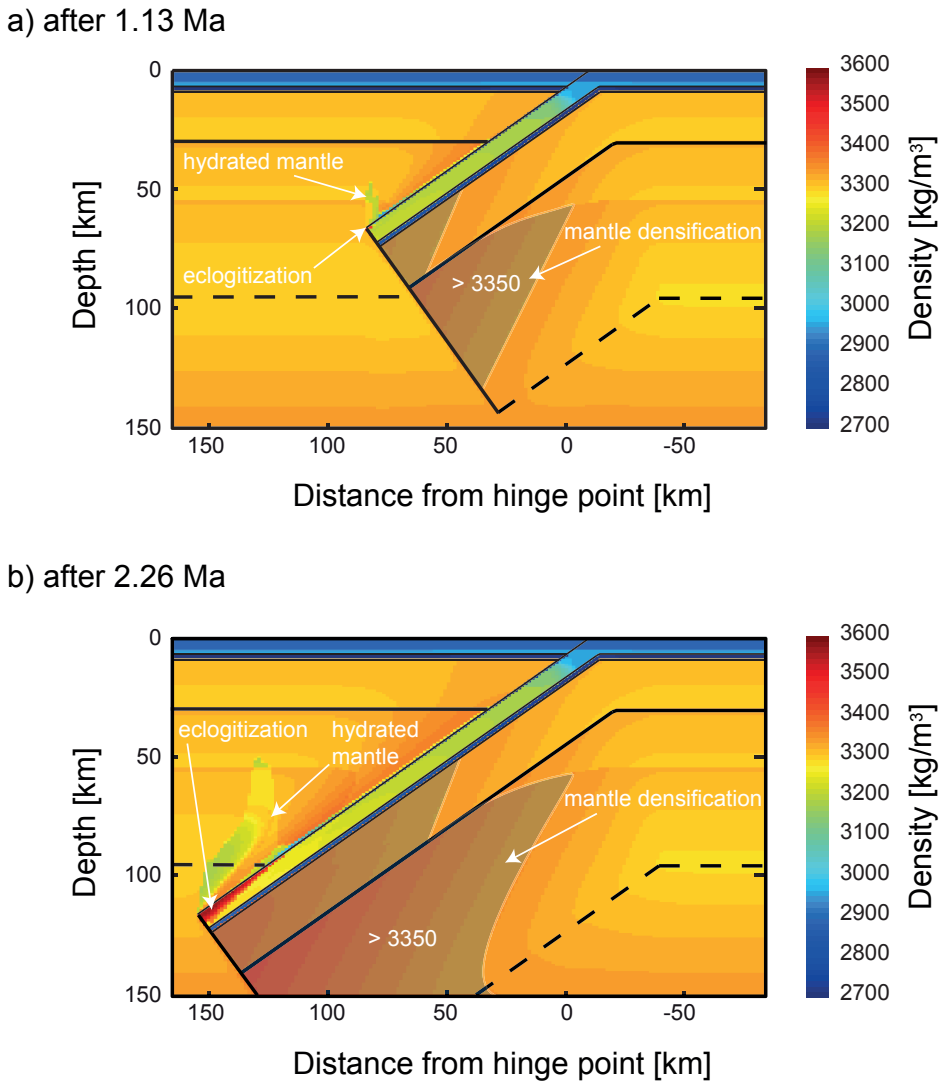

Figure 4: Density variation in a subduction zone. a) Metamorphic density in the early stage of subduction after 1.13 Ma. Note that eclogitization starts just at the tip of the slab (red color = high density, 3600 kg/m^3), whereas the lithosphere of the descending slab (shaded area ">3350 kg/m^3") is already denser than the surrounding mantle. b) After 2.26 Ma, the eclogitization of the mafic layer becomes significant (red part; 3600 kg/m^3), but the dense lithospheric portion also increases in size (shaded area). Dashed black line - base of the lithosphere.

sodium. Such a partial melt may contain a large amount of aluminum (ca. 20 mol %, see Fig. 3). Over time, the melt should become enriched in mantle-incompatible elements due to ongoing water release and fractionation. Thus, the partial melt will ultimately correspond to an approximately basaltic composition.

3.3. Impact of density changes on pressure

Assuming a constant molar mass of the rock, the metamorphic density change is reciprocal to the volume change (e.g., Heténi et al., 2011). These changes in the subducted slab will result in the generation of over- or underpressure conditions, depending on volume expansion or compression, because metamorphic reactions are either endothermic or exothermic. The Clapeyron law describes the temperature dependence of phase transitions:

$$dP/dT = \Delta H/(T\Delta V) \quad (1)$$

where ΔH and ΔV are enthalpy and the volume difference of the phase transformation, respectively, and T is the equilibrium temperature. As a result, endothermic reactions ($\Delta H < 0$) have a negative dP/dT slope with depth. The resulting positive ΔV generates overpressure conditions in the surrounding area due to the expansion of the rocks. In contrast, exothermic reactions with negative ΔV (compression) result in a zone of underpressure relative to the

ambient pressure. Zones of over- and underpressure may both trigger earthquakes if the contrast to the ambient pressure is significant (e.g., Audet et al., 2009; Green and Houston, 1995; Kato et al., 2010). Therefore, we calculate the resulting pressure difference, ΔP, by applying the ratio $P_2/P_1=V_2/V_1$:

$$\Delta P = \frac{P_1}{V_1}(V_1 + \Delta V) - P_1 \tag{2}$$

where P_1 is the ambient pressure and V_1 is the initial volume of the rock (volume from enthalpy). In the upper 250 km of the lithosphere beneath a subduction zone, there are two significant reactions with regard to density increases (i.e., volume reductions) in the crustal layer of the descending slab and in the mantle wedge beneath the overriding plate (Fig. 3).

In the crustal layer of the descending slab, a large amount of free fluid (calculated as water) is released at 3.5 GPa because most of the hydrous mineral phases (mainly chlorite and glaucophane) lose their thermodynamic stability (Fig. 3a). The release of free water results in an increase in the density of the slab lithology and thus may cause a peak underpressure in the surrounding mantle of approximately 80 MPa (Fig. 3b). The deeper reaction in the crustal layer is well known as eclogitization, where the oceanic crust of the descending slab becomes denser than the surrounding mantle due to the formation of a dense garnet-omphacite assemblage at temperatures above 400 °C (Fig. 3a). This reaction can cause a peak underpressure of approximately 90 MPa (corresponding to a rock column of ca. 3 km) and may simultaneously lead to an increase in slab pull and stretching of the slab due to the density increase of the slab (Fig. 3b). Thus, eclogitization plays a major role in the slab pull force only at a later subduction stage, assuming that our calculated *P-T* field approximately represents a realistic steady state (see 3.4).

Well-known dehydration reactions (chlorite-out; amphibole-out; garnet-in) affect the lithospheric mantle above the slab-wedge interface. Due to fluid migration (calculated as water), water will be supplied to the mantle wedge at a depth lower than 70 km (Fig. 3a), as was observed by Bostock et al. (2002). Below 800 °C, the density of the mantle wedge is significantly influenced by the newfound stability of hydrated phases, such as pargasitic amphibole and chlorite, which require free water to form (Grove et al., 2012). This reaction results in a volume expansion, causing an overpressure of up to 10 MPa (Fig. 3b). Formation of serpentine minerals (e.g., antigorite) at temperatures lower than 650 °C strongly decreases the density of the hydrated mantle wedge (Fig. 3a) because serpentine stores more H_2O (up to 13%) than denser amphibole or chlorite. Consequently, the volume increase (associated with the serpentine formation) leads to expansion, resulting in an overpressure of up to 50 MPa in the surrounding mantle (Fig. 3b). In summary, reactions accompanied by hydration or dehydration lead to large changes of volume and hence over- or underpressure induced by mineral reactions (up to 100 MPa). Conversely, local over- or underpressure could locally change the position of phase transitions in *P-T* space, although over- or underpressures lower than approximately 100 MPa will not have a significant impact on the position of phase transitions (because these would fall within the range of uncertainty of the thermodynamic data, see e.g., Bucher and Grapes, 2011).

3.4. Eclogitization at the early stages of subduction

The formation of high-density eclogite in a MORB-type slab is possible only if the rock reaches the garnet phase stability field. This process is primarily temperature driven. As a rule of thumb, a temperature of 400 (slab depth > 100 km) to 500 °C (a depth between 50 and 100 km) must be achieved to ensure the stability of garnet. The time needed to achieve HT conditions depends on the specific subduction conditions, subduction velocity and dip angle. In our model (subduction velocity: 7.7 cm/a), this time is achieved after 1.13 Ma. At this stage, eclogitization occurs at an approximate depth of 60 km (1.8 GPa) and affects only a small part of the tip of the slab (Fig. 4a). Initially, this part is too small to have a significant influence on slab pull. At this time step, the buoyancy force of the crustal part is positive (Fig. 5a). Thus, the slab has to descend to a greater depth. In the proceeding subduction, the eclogitization depth becomes deeper and is now localized at 90-120 km (Fig. 4b). At approximately 120 km (after 2.26 Ma), the area of eclogitization is large enough to generate a contribution to the slab pull forces (Fig. 5b). After 11 Ma, our subduction model reaches a thermal steady state, which implies that the eclogitization depth (ca. 180-200 km) no longer changes (Figs. 2 and 3). In comparison, a lithospheric density increase (> 3350 kg/m^3, i.e., higher than the average density of ambient mantle) is always present, even before 1.13 Ma, due to the pressure increase and temperature decrease caused by the burial of the descending slab (Fig. 4). Note that in TEMSPOL slabs remain colder than the thermo-mechanical model (see supplementary material) due to differences in the treatment of induced-flow effects and rheology (see also Bina and Kawakatsu, 2010). Consequently, the thermal steady-state eclogitization depth is located at a shallower depth in the thermo-mechanical model (ca. 150-170 km). The early stages of subduction (the first 3 Ma) are not affected, with the result that both models, the thermo-kinematic model and the thermo-mechanical model, predict similar eclogitization depths and buoyancy forces (see supplementary material).

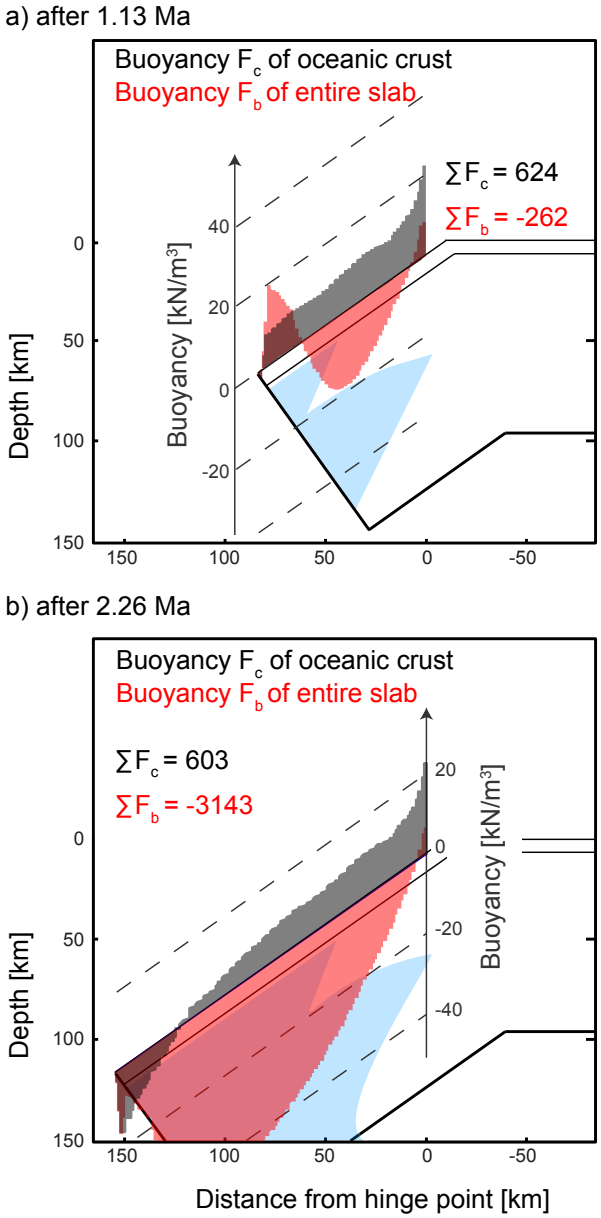

Figure 5: Buoyancies per volume unit ($g\Delta\rho$) relative to ambient mantle. The buoyancy forces correspond to Fig. 4. Positive buoyancies float; negative buoyancies sink. a) Buoyancy during the early stage of subduction after 1.13 Ma. Note that the total buoyancy of the entire slab is negative (red area), while the crust by itself is buoyant (black area). b) After 2.26 Ma, the eclogitization of the oceanic crust becomes significant, but the dense lithospheric part (blue shaded area = "$\rho > 3350$ kg/m^3") has a higher contribution to the total negative buoyancy of the entire slab.

4. Discussion

Our model is a first-order attempt to assess the metamorphic density changes during the early stages of subduction. We first model the metamorphic density under steady state and equilibrium conditions, ignoring visco-elasto-plastic behavior and assuming simple kinematic movement of the slab. The thermo-mechanical model results in similar outcomes (supplementary material), demonstrating that the results are not affected by the numerical modeling method. Additionally, the early stages of subduction are not affected by the approach of unplugged metamorphic density and flow because the flow is minor at this stage. Our results are based on thermodynamic "in situ" calculations of the metamorphic density, amount of water and partial melt (see 2). This approach differs from other density models predicted by gravity (e.g., Köther et al., 2012; Tassara and Echaurren, 2012) or pre-computed look-up tables (e.g., Afonso and Zlotnik, 2011; Bousquet et al., 1997; Doin and Henry, 2001; Duretz et al., 2012). It allows more realistic

calculation of phase transitions in *P-T-t* space and inclusion of fractionation processes. Partial melting, fractionation and mantle hydration strongly influence the density pattern of the mantle wedge. The resulting density decrease (accompanied by volume increase) may cause expansion stress of up to 50 MPa (Fig. 3b). Compared with a typical ridge push stress on the order of 20-30 MPa (assuming a lithosphere thickness of 100 km) (e.g., Forsyth and Uyeda, 1975; Schellart, 2004), this metamorphic stress is even greater. Consequently, mantle hydration results in significant forces due to expansion in the volume of the hydrated rocks in the mantle wedge and thus may affect the tectonic setting. We suggest a possible influence on subduction-related divergent stress regimes, such as cracking of/in the overriding plate allowing volcanism, a roll-back mechanism or the formation of a back-arc basin. However, assuming pure vertical fluid migration is an oversimplification and needs to be addressed (see, e.g., Wada et al., 2012). Other studies suggest that the fluid migration is driven by Darcy's law (e.g., Faccenda et al., 2012; Hebert et al., 2009b), by the fluid pressure gradient through a medium with dynamic permeability (Angiboust et al., 2012) or the effect of a slab-inward fluid migration due to the unbending of the slab (Faccenda et al., 2012). The thickness of the serpentinite layer mainly controls the amount of free fluids. The presence of a thicker serpentinite layer (e.g., 10 km) would imply a more positively buoyant slab, as well as an increase in the amount of released water. Under this assumption, we expect to observe a longer-lasting water migration process, with a greater quantity of water-saturated mantle material in the mantle wedge. This is mainly due to the greater amount of free water in the system that is absorbed by the dry mantle material. Hence, the presence of more water would reduce the density in the newly hydrated mantle wedge.

The contribution of the eclogitization of the subducted crust to the slab pull force is not crucial during the early stage of subduction (Fig. 5). We show that the increase of density of the subducted, lithospheric mantle provides a higher contribution to slab pull than the eclogitization of crustal rocks. In addition, the densification of the lithospheric mantle is a process that begins earlier than the eclogitization of the MORB layer, which becomes significant at a depth of 60-120 km (Fig. 4). Thus, the corresponding lithospheric mantle acts as additional ballast below the slab shortly after the initiation of subduction. Comparing the initiations of these two processes is a novel result, and it improves our understanding of the interaction of forces during the early stage of subduction. Such a comparison is only possible if the mineralogical phase transitions in terms of changing P-T conditions are taken into account, as presented in this study. As a matter of fact, the chemical composition of the slab is complex and variations could affect the locations (and thus timing) of phase transitions. We investigated the effect of different bulk compositions of the oceanic crust on the location (in *P-T* space) of the Garnet-in reaction (Fig. 6). Below 3 GPa, the Garnet-in reaction is almost independent of the bulk composition. Above 3 GPa, the Garnet-in reaction can vary up to 50 °C at the same pressure between an altered oceanic crust (AOC) super-composite of Kelley et al. (2003) and the average basalt composition of Hofmann (1988). In contrast, the difference between the AOC super-composite of Bach et al. (2003) and the Hofmann (1988) composition is minor (< 10 °C). In addition, Ca-rich or Fe-rich fluid flows could also influence the bulk composition of the oceanic crust but are too local to be the subject of our work. Consequently, differences in the bulk chemical composition of the oceanic crust do not have a significant influence on the outcome of this study.

Changing the model settings in terms of subduction velocity, dip angle and slab age renders our model applicable to different subduction zones. In this context, these parameters will affect the *P-T* field; thus, the eclogitization stage may occur at shallower or greater depths than in our scenario of a young, shallow, fast subduction zone. For example, in a "Lesser Antilles Scenario" (old, steep, slow, Φ = 1377 km), eclogitization takes place at a depth of 50 km (instead of 60 km) and becomes significant at approximately 100 km (instead of 120 km). However, mantle densification of the sinking slab also increases significantly at approximately 50 km and contributes more to the slab pull in this different setting. The principle effects remain the same. If the major part of the oceanic crust is eclogitized, the oceanic crust remains denser than the mantle, even near the core mantle boundary (Ricard et al., 2005).

Although the reliability of the thermodynamic databases may be problematic in regard to the implementation of melts or solid solutions, their application demonstrates the importance of interactions between the rock composition and the molar ratios of minerals, phase transitions and density. The improvement of a reliable melt model is a challenge to future studies and requires more experiments. We improved the water component of a melt solid solution of Holland and Powell (1998) but still encountered problems with the fayalite component. Without experiments at elevated temperatures and pressures, the adjustment of thermodynamic data is speculative. The use of different databases may result in different mineral assemblages and densities due to different methods (e.g., volume equation of state) and different modes of phases and solid solutions. When calculating metamorphic densities, it is crucial to cross-check predicted densities, volumes and mineral assemblages with experimental data and field petrology.

Our model could be more realistic in future studies, if refined. For example, it is obvious that the residual unhydrated part of the mantle wedge in our model should also be hydrated because the dehydration of the slab has also been present during the previous time steps (see Fig. 4). It will be a future task to compute fluid transfer and corresponding compositional changes in time.

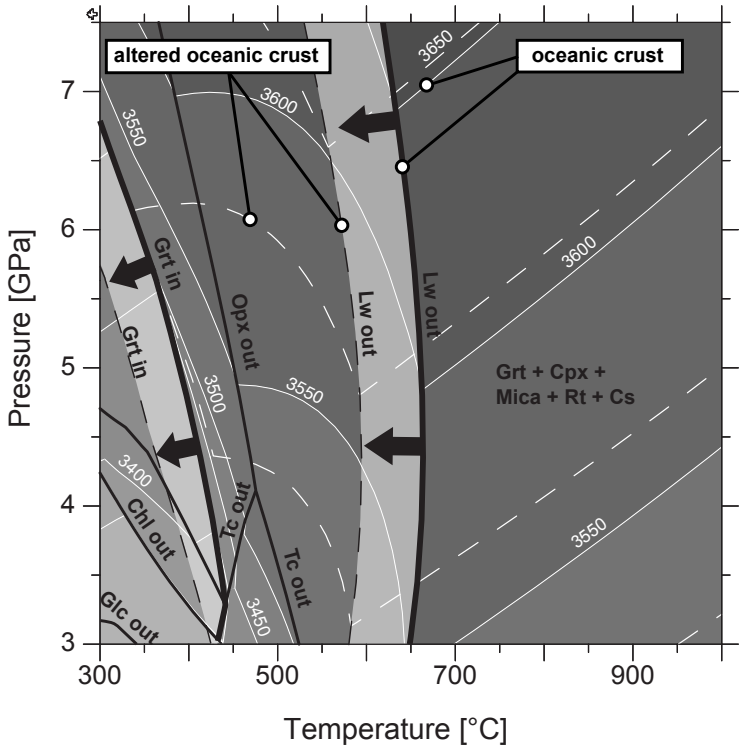

Figure 6: Phase diagram (*solid black lines*) and density isolines (*solid white lines*) for averaged oceanic crust (Hofmann, 1988) at high pressure. *Dashed white* density isolines and the low-temperature Grt-in and Lw-out reaction line (*dashed black*) correspond to the altered oceanic crust (AOC) super-composite of Kelley et al. (2003). The figure shows the effect of different bulk compositions on the location (in *P-T* space) of the Grt-in and Lw-out reaction line. For the sake of illustration, the Grt-in and Lw-out reaction line and density isoline in the range of 3500 to 3650 kg/m^3 are only shown for the altered oceanic crust. Mineral abbreviations: Chl - chlorite, Cpx - clinopyroxene, Cs - coesite, Glc - glaucophane, Grt - garnet, Lw - lawsonite, Mica - white mica, Opx - orthopyroxene, Rt - rutile, Tc - talc.

5. Conclusions

We have presented herein a study of the influence that mineralogy has on density in subduction zones. To do this, a novel approach was developed, in which we coupled state-of-the-art thermodynamic models with thermo-kinematic/mechanical models. We were able to calculate the compositions of melts and residues and the effects of phase transitions, slab dehydration and partial melting on the solid-rock densities of the slab and mantle wedge. The resulting density changes may cause maximum overpressure that is twice as large as a typical ridge push stress in the mantle wedge, which may initiate subduction-related divergent tectonics. Compared to the use of physical densities (which ignore phase transitions), our approach using metamorphic densities is a step forward in understanding subduction and related processes and makes a contribution to the improvement of other subduction models, both gravitational and numerical in nature.

Our results reveal that the mantle densification of the sinking slab provides a higher contribution to slab pull during the early stages of subduction than the eclogitization of the oceanic crust, which becomes more important during later time steps (here, after 2 Ma). We show that in the proposed setup, after 1 Ma, the entire slab is not buoyant, whereas the crust by itself is buoyant at all depths and provides no contribution to the slab pull. After 2 Ma, the crust is still buoyant and only a small portion of the tip contributes to the slab pull. Consequently, the lithospheric mantle densification occurs earlier than the eclogitization of the oceanic crust and thus dominates the early stages of subduction. Although the presented approach has some limitations, its application shows that the evolution of subduction zones can only be assessed reliably if metamorphic processes are taken into account. Indeed, “in situ” density calculations as performed here enhance our understanding of the timing and extent of the influence of metamorphic processes on the dynamics of subduction zones.

Acknowledgements

The research was supported by DFG research grant SPP 1257 project 6.2. and the Graduate School GRK1364 Shaping Earth's Surface in a Variable Environment funded by the German Research Foundation (DFG), co-financed by the federal state of Brandenburg and the University of Potsdam. We thank Olivier Vanderhaeghe and an anonymous colleague for their positive reviews, which helped to improve the quality of this manuscript.

Appendix A. Supplementary material

Appendix A.1. Thermodynamic melt model

As explained in the main article, the melt model of the tcdb55-database was modified. We updated the thermodynamic data for the water component "LIQtc_h2O" of the tcdb55 database ("h2oL" in Holland and Powell, 1998) and the corresponding Margules parameter. The updated data are presented in Table A.1. The new "LIQtc_h2o" melt species results in more realistic densities and melt stability fields. Copy and replace the values in the original tcdb55 database to apply the modified melt model.

Table A.1: Modified thermodynamic data of H2O.liq phase in the tcdb55 database of the Theriak/Domino software (de Capitani and Petrakakis, 2010)

***** GAS DATA *****					
H2O.liq	O(1)H(2)	h2oL	1nh		
ST	0.0	-107000.00	237.4385	1.3620	
C3	-20.0	0.0	0.0	10.0	0.0
VHP	0.001189	60.0	0.0	0.0	0.0
VH2	10.0	4.0	-0.00043		
***** MARGULES PARAMETER *****					
Silica8.liq - H2O.liq					
12	-29000.0	0.0	0.0		
!					
albite.liq - H2O.liq					
12	-108000.0	0.0	-0.20		
!					
K-feldspar.liq - H2O.liq					
12	-81000.0	0.0	-0.45		
!					
anorthite.liq - H2O.liq					
12	-68000.0	0.0	-0.85		
!					
sillimanite8.liq - H2O.liq					
12	-25000.0	0.0	0.0		
!					
forsterite8.liq - H2O.liq					
12	-41000.0	0.0	0.0		
!					
fayalite8.liq - H2O.liq					
12	-64000.0	0.0	0.0		

Appendix A.2. Thermo-mechanical model

An improved version of the code SLIM-3D (Quinteros and Sobolev, 2013; Quinteros et al., 2010; Popov and Sobolev, 2008) was used to run all experiments.

The finite element method (FEM) was used to solve the governing equations. Namely, the conservation of momentum

$$\frac{\partial \sigma_{ij}}{\partial x_j} + \rho \vec{g} = 0 \tag{A.1}$$

and conservation of energy

$$\rho C_p \frac{DT_P}{Dt} = \kappa \nabla^2 T_P + r \ . \tag{A.2}$$

where σ_{ij} is the Cauchy stress tensor, ρ is density, $\vec{g}$ is gravity acceleration, C_p is heat capacity, κ is thermal conductivity, $\frac{D}{Dt}$ is the material time derivative, T_P is the potential temperature and r is the volumetric heat sources.

The effects of compressibility are coupled with the constitutive equation by means of

$$\frac{Dp}{Dt} = -K\left(\frac{\partial v_i}{\partial x_i} - \alpha \frac{DT}{Dt}\right). \tag{A.3}$$

Here, K is the bulk modulus and α is the thermal expansion.

Total deviatoric strain rate ($\dot{\varepsilon}_{ij}$) is additively decomposed into an elastic, a viscous and a plastic term as follows:

$$\dot{\varepsilon}_{ij} = \dot{\varepsilon}_{ij}^{el} + \dot{\varepsilon}_{ij}^{vis} + \dot{\varepsilon}_{ij}^{pl} = \frac{\hat{\tau}_{ij}}{2G} + \frac{\tau_{ij}}{2\mu_{eff}} + \dot{\gamma}\frac{\partial Q}{\partial \tau_{ij}} \tag{A.4}$$

where G is the elastic shear modulus, μ_{eff} is the effective viscosity, $\hat{\tau}_{ij}$ is the objective stress rate tensor, $\dot{\gamma}$ is the plastic multiplier and Q is the plastic potential function. The numerical integration of stresses was calculated by means of the Hughes-Winget scheme (Hughes and Winget, 1980) for the trial stresses, whereas a predictor-corrector procedure (Simo and Taylor, 1985) was applied to update the deviatoric stresses considering plasticity.

Viscosity is stress and temperature dependent. Three different types of creep were included, following the approach of Kameyama et al. (1999).

The effective viscous strain rate was additively decomposed into three different types of creep mechanisms (diffusion, dislocation and Peierls), namely

$$\dot{\varepsilon}_{eff}^{(v)} = \dot{\varepsilon}_d + \dot{\varepsilon}_n + \dot{\varepsilon}_p \ . \tag{A.5}$$

Strain rate due to diffusion creep was defined as

$$\dot{\varepsilon}_d = B_d \tau_{II} e^{-\frac{H_d}{RT}} \ , \tag{A.6}$$

dislocation, power-law creep as

$$\dot{\varepsilon}_n = B_n \tau_{II}^n e^{-\frac{H_n}{RT}} \ , \tag{A.7}$$

and Peierls creep as

$$\dot{\varepsilon}_p = B_p e^{\left[-\frac{H_p}{RT}\left(1-\frac{\tau_{II}}{\tau_p}\right)^q\right]} \ , \tag{A.8}$$

where τ_{II} is the square root of the second invariant of the deviatoric stress; R is the gas constant; B_d, B_n, B_p are creep parameters and τ_p is Peierls stress. H_d, H_n, H_p are the activation enthalpies for each creep, which are defined as

$$H_j = E_j + P.V_j \tag{A.9}$$

for $j \in \{d, n, p\}$ and E represents the activation energy, P the pressure and V the activation volume. A yield stress (350 MPa or 500 MPa) was also applied in the transition zone and the lower mantle.

Finally, effective viscosity was calculated as

$$\mu_{eff} = \frac{\tau_{II}}{2\dot{\varepsilon}_{eff}^{(v)}} \ . \tag{A.10}$$

We used wet olivine parameters for the rheology of the upper mantle (Hirth and Kohlstedt, 2003). All the experiments were run with a coarser and a finer grid (1000 x 335 and 1400 x 660 elements, respectively). The average size of the finer element is $\sim 1.0 \times 1.0\ km^2$.

The resulting density (Fig. A.1) and buoyancy calculations (Fig. A.2) are shown for comparison with the thermokinematic model of the main article. It is shown that the outputs of the two modeling approaches are similar. Consequently, the figures make clear that the densification of the lithospheric mantle of the sinking slab starts earlier than the eclogitization of the crust and provides a higher contribution to slab pull.

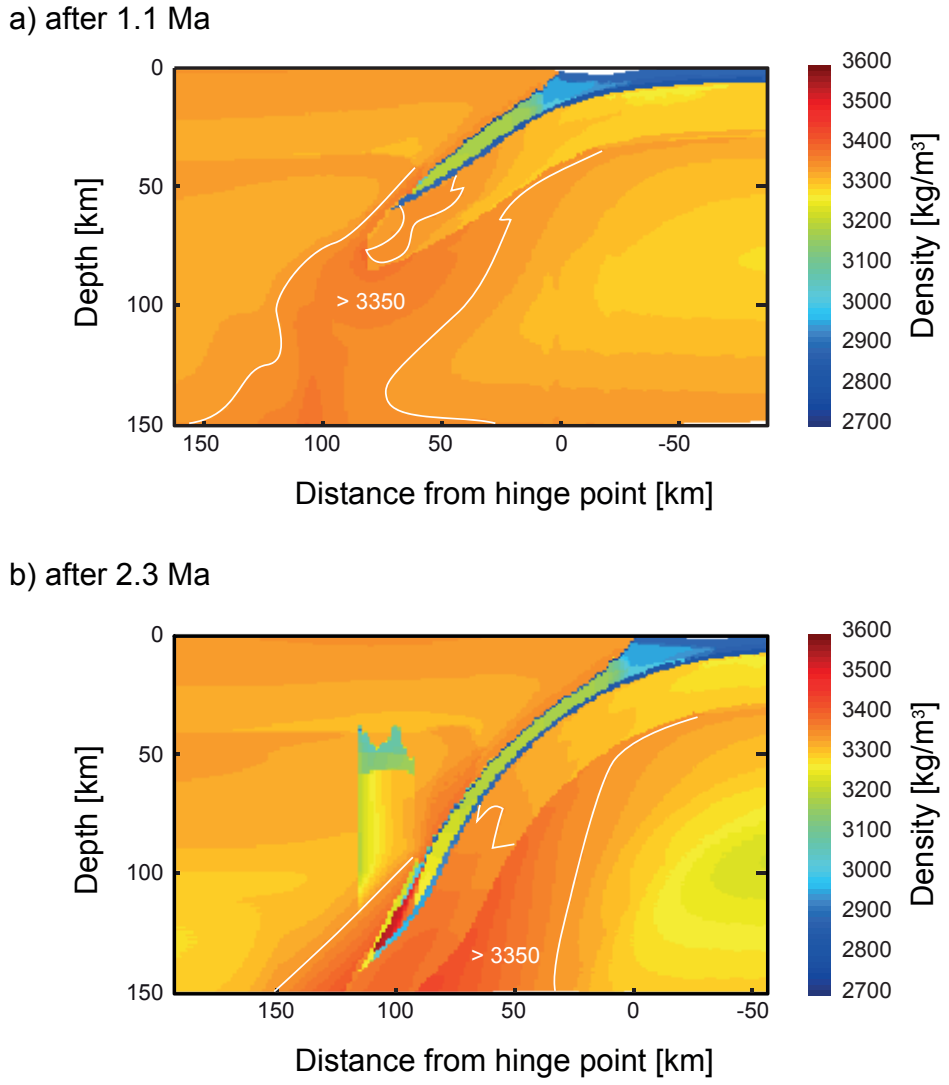

Figure A.1: Density variations in a subduction zone. a) Metamorphic density during the early stage of subduction after 1.1 Ma. Note that eclogitization has not begun, whereas the lithosphere of the descending slab (area ">3350 kg/m^3") is already denser than the surrounding mantle. b) After 2.3 Ma, the eclogitization of the mafic layer becomes significant (red part; 3600 kg/m^3), but the dense lithospheric part also increases in size (area labeled ">3350 kg/m^3").

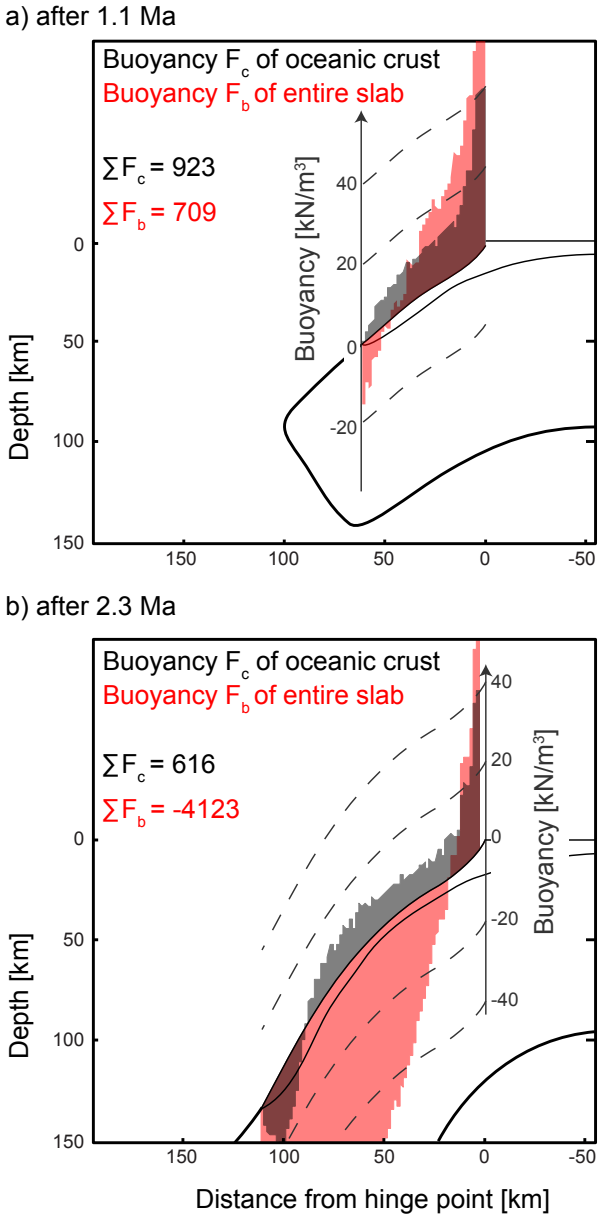

Figure A.2: Buoyancies per volume unit ($g\Delta\rho$) relative to ambient mantle. Buoyancy forces correspond to Fig. A.1. Positive buoyancies float; negative buoyancies sink. a) Buoyancy during the early stage of subduction after 1.1 Ma. Note that the buoyancy of the entire slab (red area) becomes negative due to mantle densification. b) After 2.3 Ma, the eclogitization of the oceanic crust becomes significant, but the dense lithospheric part has a higher contribution to the total negative buoyancy of the entire slab.

Afonso, J., Ranalli, G., Fernandez, M., 2005. Thermal expansivity and elastic properties of the lithospheric mantle: results from mineral physics of composites. Physics of the Earth and Planetary Interiors 149, 279–306. doi:10.1016/j.pepi.2004.10.003.

Afonso, J.C., Zlotnik, S., 2011. The subductability of continental lithosphere: The before and after story, in: Brown, D., Ryan, P.D. (Eds.), Arc-Continent Collision. Springer Verlag, Berlin, Heidelberg. Frontiers in Earth Sciences. chapter 3, pp. 53–86. doi:10.1007/978-3-540-88558-0.

Angiboust, S., Wolf, S., Burov, E., Agard, P., Yamato, P., 2012. Effect of fluid circulation on subduction interface tectonic processes: Insights from thermo-mechanical numerical modelling. Earth and Planetary Science Letters 357-358, 238–248. doi:10.1016/j.epsl.2012.09.012.

Arcay, D., Tric, E., Doin, M., 2005. Numerical simulations of subduction zones: Effect of slab dehydration on the mantle wedge dynamics. Physics of The Earth and Planetary Interiors 149, 133–153. doi:10.1016/j.pepi.2004.08.020.

Audet, P., Bostock, M.G., Christensen, N.I., Peacock, S.M., 2009. Seismic evidence for overpressured subducted oceanic crust and megathrust fault sealing. Nature 457, 76–78. doi:10.1038/nature07650.

Babeyko, A.Y., Sobolev, S.V., 2008. High-resolution numerical modeling of stress distribution in visco-elasto-plastic subducting slabs. Lithos 103, 205–216. doi:10.1016/j.lithos.2007.09.015.

Bach, W., Peucker-Ehrenbrink, B., Hart, S.R., Blusztajn, J.S., 2003. Geochemistry of hydrothermally altered oceanic crust: DSDP/ODP Hole 504B - Implications for seawater-crust exchange budgets and Sr- and Pb-isotopic evolution of the mantle. Geochemistry, Geophysics, Geosystems 4, 1–29. doi:10.1029/2002GC000419.

Berman, R., 1988. Internally-consistent thermodynamic data for minerals in the system Na2O-K2O-CaO-MgO-FeO-Fe2O3-Al2O3-SiO2-TiO2-H2O-CO2. Journal of Petrology 29, 445–552.

Billen, M.I., 2008. Modeling the dynamics of subducting slabs. Annual Review of Earth and Planetary Sciences 36, 325–356. doi:10.1146/annurev.earth.36.031207.124129.

Bina, C.R., Kawakatsu, H., 2010. Buoyancy, bending, and seismic visibility in deep slab stagnation. Physics of the Earth and Planetary Interiors 183, 330–340. doi:10.1016/j.pepi.2010.04.010.

Bina, C.R., Stein, S., Marton, F.C., Van Ark, E.M., 2001. Implications of slab mineralogy for subduction dynamics. Physics of the Earth and Planetary Interiors 127, 51–66. doi:10.1016/S0031-9201(01)00221-7.

Bostock, M.G., Hyndman, R.D., Rondenay, S., Peacock, S.M., 2002. An inverted continental Moho and serpentinization of the forearc mantle. Nature 417, 536–538. doi:10.1038/417536a.

Bousquet, R., Goffé, B., Henry, P., Le Pichon, X., Chopin, C., 1997. Kinematic, thermal and petrological model of the Central Alps: Lepontine metamorphism in the upper crust and eclogitisation of the lower crust. Tectonophysics 273, 105–127. doi:10.1016/S0040-1951(96)00290-9.

Bousquet, R., Goffé, B., Le Pichon, X., de Capitani, C., Chopin, C., Henry, P., 2005. Comment on "Subduction factory: 1. Theoretical mineralogy, densities, seismic wave speeds, and H2O contents" by Bradley R. Hacker, Geoffrey A. Abers, and Simon M. Peacock. Journal of Geophysical Research 110, 1–3. doi:10.1029/2004JB003450.

Brown, G.C., Mussett, A.E., 1993. The inaccessible earth: an integrated view of its structure and composition. 2 ed., Chapman & Hall, London.

Bucher, K., Grapes, R., 2011. Petrogenesis of Metamorphic Rocks. 8 ed., Springer, Berlin Heidelberg.

de Capitani, C., Brown, T., 1987. The computation of chemical equilibrium in complex systems containing non-ideal solutions. Geochimica et Cosmochimica Acta 51, 2639–2652.

de Capitani, C., Petrakakis, K., 2010. The computation of equilibrium assemblage diagrams with Theriak/Domino software. American Mineralogist 95, 1006–1016. doi:10.2138/am.2010.3354.

Connolly, J., Kerrick, D., 2002. Metamorphic controls on seismic velocity of subducted oceanic crust at 100–250 km depth. Earth and Planetary Science Letters 204, 61–74. doi:10.1016/S0012-821X(02)00957-3.

Davies, J.H., 1999. The role of hydraulic fractures and intermediate-depth earthquakes in generating subduction-zone magmatism. Nature 398, 142–145. doi:10.1038/18202.

Doin, M., Henry, P., 2001. Subduction initiation and continental crust recycling: the roles of rheology and eclogitization. Tectonophysics 342, 163–191.

Duesterhoeft, E., Bousquet, R., Wichura, H., Oberhänsli, R., 2012. Anorogenic plateau formation: The importance of density changes in the lithosphere. Journal of Geophysical Research 117, 1–13. doi:10.1029/2011JB009007.

Duesterhoeft, E., de Capitani, C., 2013. THERIAK_D: an add-on to implement equilibrium computations in geodynamic models. Geochemistry, Geophysics, Geosystems 14, 4962–4967. doi:10.1002/ggge.20286.

Duesterhoeft, E., 2013. The impact of metamorphic processes on physical properties: A view from thermodynamics to geodynamics. PhD thesis, University of Potsdam.

Duretz, T., Gerya, T.V., Kaus, B.J.P., Andersen, T.B., 2012. Thermomechanical modeling of slab eduction. Journal of Geophysical Research 117, 1–17. doi:10.1029/2012JB009137.

Ellis, D.E., Wyllie, P.J., 1979. Hydration and melting reactions in the system MgO-SiO2-H2O at pressures up to 100 kbar. American Mineralogist 64, 41–48.

Faccenda, M., Gerya, T.V., Mancktelow, N.S., Moresi, L., 2012. Fluid flow during slab unbending and dehydration: Implications for intermediate-depth seismicity, slab weakening and deep water recycling. Geochemistry, Geophysics, Geosystems 13, 1–23. doi:10.1029/2011GC003860.

Forsyth, D., Uyeda, S., 1975. On the relative importance of the driving forces of plate motion. Geophysical Journal of the Royal Astronomical Society 43, 163–200.

Ganguly, J., Freed, A., Saxena, S., 2009. Density profiles of oceanic slabs and surrounding mantle: Integrated thermodynamic and thermal modeling, and implications for the fate of slabs at the 660 km discontinuity. Physics of the Earth and Planetary Interiors 172, 257–267. doi:10.1016/j.pepi.2008.10.005.

Gerya, T., 2011. Future directions in subduction modeling. Journal of Geodynamics 52, 344–378. doi:10.1016/j.jog.2011.06.005.

Gerya, T.V., Connolly, J.A.D., Yuen, D.A., 2008. Why is terrestrial subduction one-sided? Geology 36, 43–46. doi:10.1130/G24060A.1.

Gerya, T.V., Stöckhert, B., Perchuk, A.L., 2002. Exhumation of high-pressure metamorphic rocks in a subduction channel: A numerical simulation. Tectonics 21, 1056. doi:10.1029/2002TC001406.

Gerya, T.V., Yuen, D.A., Maresch, W.V., 2004. Thermomechanical modelling of slab detachment. Earth and Planetary Science Letters 226, 101–116. doi:10.1016/j.epsl.2004.07.022.

Ghiorso, M.S., Hirschmann, M.M., Reiners, P.W., 2002. The pMELTS: A revision of MELTS for improved calculation of phase relations and major element partitioning related to partial melting of the mantle to 3 GPa. Geochemistry Geophysics Geosystems 3, 1–36.

Giunchi, C., Ricard, Y., 1999. High-pressure/low-temperature metamorphism and the dynamics of an accretionary wedge. Geophysical Journal International 136, 620–628. doi:10.1046/j.1365-246x.1999.00759.x.

Goffé, B., Bousquet, R., Henry, P., Le Pichon, X., 2003. Effect of the chemical composition of the crust on the metamorphic evolution of orogenic

wedges. Journal of Metamorphic Geology 21, 123–141. doi:10.1046/j.1525-1314.2003.00422.x.
Green, H.I., Houston, H., 1995. The mechanics of deep earthquakes. Annual Review of Earth and Planetary Sciences 23, 169–213.
Grove, T.L., Till, C.B., Krawczynski, M.J., 2012. The Role of H2O in Subduction Zone Magmatism. Annual Review of Earth and Planetary Sciences 40, 413–439. doi:10.1146/annurev-earth-042711-105310.
Guillot, S., Hattori, K., Agard, P., Schwartz, S., Vidal, O., 2009. Exhumation processes in oceanic and continental subduction contexts: a review, in: Lallemand, S., Funiciello, F. (Eds.), Subduction Zone Geodynamics. Springer, Berlin, Heidelberg. Frontiers in Earth Sciences, pp. 175–205. doi:10.1007/978-3-540-87974-9.
Hacker, B.R., 2008. H2O subduction beyond arcs. Geochemistry, Geophysics, Geosystems 9, 1–24. doi:10.1029/2007GC001707.
Hacker, B.R., Abers, G.A., Peacock, S.M., 2003. Subduction factory 1. Theoretical mineralogy, densities, seismic wave speeds, and H2O contents. Journal of Geophysical Research 108, 1–26. doi:10.1029/2001JB001127.
Hebert, L.B., Antoshechkina, P., Asimow, P., Gurnis, M., 2009a. Emergence of a low-viscosity channel in subduction zones through the coupling of mantle flow and thermodynamics. Earth and Planetary Science Letters 278, 243–256. doi:10.1016/j.epsl.2008.12.013.
Hebert, L.B., Asimow, P., Antoshechkina, P., 2009b. Fluid source-based modeling of melt initiation within the subduction zone mantle wedge: Implications for geochemical trends in arc lavas. Chemical Geology 266, 306–319. doi:10.1016/j.chemgeo.2009.06.017.
Henry, P., Le Pichon, X., Goffé, B., 1997. Kinematic, thermal and petrological model of the Himalayas: constraints related to metamorphism within the underthrust Indian crust and topographic elevation. Tectonophysics 273, 31–56.
Hetényi, G., Godard, V., Cattin, R., Connolly, J., 2011. Incorporating metamorphism in geodynamic models: the mass conservation problem. Geophysical Journal International 186, 6–10. doi:10.1111/j.1365-246X.2011.05052.x.
Hirth, G., Kohlstedt, D.L., 2003. Rheology of the upper mantle and the mantle wedge: A view from the experimentalists, in: Eiler, J. (Ed.), Inside the Subduction Factory. American Geophysical Union. volume 138 of *Geophysical Monograph*, pp. 83–105.
Hofmann, A.W., 1988. Chemical differentiation of the Earth: the relationship between mantle, continental crust, and oceanic crust. Earth and Planetary Science Letters 90, 297–314. doi:10.1016/0012-821X(88)90132-X.
Holland, T., Powell, R., 1998. An internally consistent thermodynamic data set for phases of petrological interest. Journal of Metamorphic Geology 16, 309–343.
Hughes, T.J.R., Winget, J., 1980. Finite rotation effects in numerical integration of rate constitutive equations arising in large-deformation analysis. International Journal for Numerical Methods for Engineering 15, 1862–1867.
Isacks, B , Oliver, J ,Sykes, L.R. 1968. Seismology and the new global tectonics. Journal of Geophysical Research 73, 5855–5899.
Jaupart, C., Mareschal, J.C., 2011. Heat Generation and Transport in the Earth. Cambridge University Press, Cambridge, U.K.
John, T., Gussone, N., Podladchikov, Y.Y., Bebout, G.E., Dohmen, R., Halama, R., Klemd, R., Magna, T., Seitz, H.M., 2012. Volcanic arcs fed by rapid pulsed fluid flow through subducting slabs. Nature Geoscience 5, 489–492. doi:10.1038/ngeo1482.
Kameyama, M., Yuen, D.A., Karato, S., 1999. Thermal-mechanical effects on low-temperature plasticity (the Peierls mechanism) on the deformation of a viscoelastic shear zone. Earth and Planetary Science Letters 168, 159–172.
Kárason, H., Van der Hilst, R.D., 2002. Constraints on mantle convection from seismic tomography. Geophysical Monograph 121, 277–288.
Kato, A., Iidaka, T., Ikuta, R., Yoshida, Y., Katsumata, K., Iwasaki, T., Sakai, S., Thurber, C., Tsumura, N., Yamaoka, K., Watanabe, T., Kunitomo, T., Yamazaki, F., Okubo, M., Suzuki, S., Hirata, N., 2010. Variations of fluid pressure within the subducting oceanic crust and slow earthquakes. Geophysical Research Letters 37, 1–5. doi:10.1029/2010GL043723.
Kawamoto, T., Holloway, J., 1997. Melting Temperature and Partial Melt Chemistry of H2O-Saturated Mantle Peridotite to 11 Gigapascals. Science 276, 240–243.
van Keken, P.E., Currie, C., King, S.D., Behn, M.D., Cagnioncle, A., He, J., Katz, R.F., Lin, S.C., Parmentier, E.M., Spiegelman, M., Wang, K., 2008. A community benchmark for subduction zone modeling. Physics of the Earth and Planetary Interiors 171, 187–197. doi:10.1016/j.pepi.2008.04.015.
Kelley, K.A., Plank, T., Ludden, J., Staudigel, H., 2003. Composition of altered oceanic crust at ODP Sites 801 and 1149. Geochemistry, Geophysics, Geosystems 4, 1–21. doi:10.1029/2002GC000435.
Köther, N., Götze, H.J., Gutknecht, B., Jahr, T., Jentzsch, G., Lücke, O., Mahatsente, R., Sharma, R., Zeumann, S., 2012. The seismically active Andean and Central American margins: Can satellite gravity map lithospheric structures? Journal of Geodynamics 59-60, 207–218. doi:10.1016/j.jog.2011.11.004.
Le Pichon, X., 1968. Sea-floor spreading and continental drift. Journal of Geophysical Research 73, 3661–3697.
Le Pichon, X., Henry, P., Goffé, B., 1997. Uplift of Tibet: from eclogites to granulites—implications for the Andean Plateau and the Variscan belt. Tectonophysics 273, 57–76.
Lee, C.T.A., Chen, W.P., 2007. Possible density segregation of subducted oceanic lithosphere along a weak serpentinite layer and implications for compositional stratification of the Earth's mantle. Earth and Planetary Science Letters 255, 357–366. doi:10.1016/j.epsl.2006.12.022.
Li, Z. H., Gerya, T. V., Burg, J.-P. 2010. Influence of tectonic overpressure on P-T paths of HP-UHP rocks in continental collision zones: thermomechanical modelling. Journal of Metamorphic Geology 28, 227–247. doi:10.1111/j.1525-1314.2009.00864.x.
Li, X.P., Rahn, M., Bucher, K., 2004. Serpentinites of the Zermatt-Saas ophiolite complex and their texture evolution. Journal of Metamorphic Geology 22, 159–177. doi:10.1111/j.1525-1314.2004.00503.x.
McKenzie, D.P., 1969. Speculations on the Consequences and Causes of Plate Motions*. Geophysical Journal of the Royal Astronomical Society 18, 1–32.
Morgan, W.J., 1968. Rises, trenches, great faults, and crustal blocks. Journal of Geophysical Research 73, 1959–1982.
Negredo, A., Valera, J., Carminati, E., 2004. TEMSPOL: a MATLAB thermal model for deep subduction zones including major phase transformations. Computers & Geosciences 30, 249–258. doi:10.1016/j.cageo.2004.01.002.
Oxburgh, E.R., Parmentier, E.M., 1977. Compositional and density stratification in oceanic lithosphere-causes and consequences. Journal of the Geological Society 133, 343–355. doi:10.1144/gsjgs.133.4.0343.
Peacock, S.M., 1987. Thermal effects of metamorphic fluids in subduction zones. Geology 15, 1057–1060. doi:10.1130/0091-7613(1987)15¡1057.
Peacock, S.M., 1996. Subduction Top to Bottom. Geophysical Monograph Series 96, 119–133. doi:10.1029/GM096.
Petrini, K., Podladchikov, Y., 2000. Lithospheric pressure-depth relationship in compressive regions of thickned crust. Journal of Metamorphic Geology 18, 67–77.
Poli, S., Schmidt, M.W., 2002. Petrology of subducted slabs. Annual Review of Earth and Planetary Sciences 30, 207–235. doi:10.1146/annurev.earth.30.091201.140550.
Popov, A.A., Sobolev, S.V., 2008. Slim3d: A tool for three-dimensional thermomechanical modeling of the lithospheric deformation with elasto-visco-plastic rheology. Physics of the Earth Interiors 171, 55–75. doi:10.1016/j.pepi.2008.03.007.

Pourteau, A., Candan, O., Oberhänsli, R., 2010. High-pressure metasediments in central Turkey: Constraints on the Neotethyan closure history. Tectonics 29, 1–18. doi:10.1029/2009TC002650.

Prezzi, C.B., Götze, H.J., Schmidt, S., 2009. 3D density model of the Central Andes. Physics of the Earth and Planetary Interiors 177, 217–234. doi:10.1016/j.pepi.2009.09.004.

Quinteros, J., Sobolev, S.V., 2012. Constraining kinetics of metastable olivine in the Marianas slab from seismic observations and dynamic models. Tectonophysics 526-529, 48–55. doi:10.1016/j.tecto.2011.11.005.

Quinteros, J., Sobolev, S.V., 2013. Why has the Nazca plate slowed since the Neogene? Geology 41, 31–34. doi:10.1130/G33497.1.

Quinteros, J., Sobolev, S.V., Popov, A.A., 2010. Viscosity in transition zone and lower mantle. Implications for slab penetration. Geophysical Research Letters 37, L09307. doi:10.1029/2010GL043140.

Raz, U., Girsperger, S., Thompson, A.B., 2002. Thermal expansion, compressibility and volumetric changes of quartz obtained by single crystal dilatometry to 700 °C and 3.5 kilobars (0.35 GPa). Schweizerische Mineralogische und Petrographische Mitteilungen 82, 561–574. doi:10.3929/ethz-a-004392716.

Ricard, Y., Mattern, E., Matas, J., 2005. Synthetic tomographic images of slabs from mineral physics, in: van der Hilst, R., Bass, J.D., Matas, J., Trampert, J. (Eds.), Earth's Deep Mantle: Structure, Composition, and Evolution, Geophysical Monograph Series. AGU, Washington, D. C.. volume 160, pp. 283–300. doi:10.1029/160GM17.

Ringwood, A., Green, D., 1966. An experimental investigation the gabbro-eclogite transformation and some geophysical implications. Tectonophysics 3, 383–427.

Ringwood, A., Irifune, T., 1988. Nature of the 650-km seismic discontinuity: implications for mantle dynamics and differentiation. Nature 331, 131–136.

Robie, R.A., Hemingway, B.S., 1995. Thermodynamic properties of minerals and related substances at 298.15 K and 1 bar (10ˆ5 Pascals) pressure and at higher temperatures. U.S. Geological Survey Bulletin 2131, 461.

Rüpke, L.H., Morgan, J.P., Hort, M., Connolly, J.A.D., Ru, L.H., 2002. Are the regional variations in Central American arc lavas due to differing basaltic versus peridotitic slab sources of fluids ? Geology 30, 1035–1038. doi:10.1130/0091-7613(2002)030¡1035.

Schellart, W.P., 2004. Quantifying the net slab pull force as a driving mechanism for plate tectonics. Geophysical Research Letters 31, L07611. doi:10.1029/2004GL019528.

Schmidt, M., Poli, S., 1998. Experimentally based water budgets for dehydrating slabs and consequences for arc magma generation. Earth and Planetary Science Letters 163, 361–379.

Simo, J.C., Taylor, R.L., 1985. Consistent tangent operators for rate-independent elasto-plasticity. Computer Methods in Applied Mechanics and Engineering 48, 101–118.

Simon, N.S., Podladchikov, Y.Y., 2008. The effect of mantle composition on density in the extending lithosphere. Earth and Planetary Science Letters 272, 148–157. doi:10.1016/j.epsl.2008.04.027.

Sobolev, S.V., Babeyko, A.Y., 1994. Modeling of mineralogical composition, density and elastic wave velocities in anhydrous magmatic rocks. Surveys in Geophysics 15, 515–544. doi:10.1007/BF00690173.

Sobolev, S.V., Babeyko, A.Y., 2005. What drives orogeny in the Andes? Geology 33, 617–620.

Sobolev, S.V., Babeyko, A.Y., Koulakov, I., Oncken, O., 2006. Mechanism of the Andean Orogeny: Insight from Numerical Modeling, in: Oncken, O., Chong, G., Franz, G., Giese, P., Götze, H.J., Ramos, V.A., Strecker, M.R., Wigger, P. (Eds.), The Andes Frontiers in Earth Sciences. Springer, Berlin Heidelberg. chapter Part IV, pp. 513–535. doi:10.1007/978-3-540-48684-8_25.

Stein, C., Stein, S., 1992. A model for the global variation in oceanic depth and heat flow with lithospheric age. Nature 359, 123–129.

Stern, R.J., 2002. Subduction zones. Reviews of Geophysics 40, 1012. doi:10.1029/2001RG000108.

Tassara, A., Echaurren, A., 2012. Anatomy of the Andean subduction zone: three-dimensional density model upgraded and compared against global-scale models. Geophysical Journal International 189, 161–168. doi:10.1111/j.1365-246X.2012.05397.x.

Tašárová, Z.A., 2007. Towards understanding the lithospheric structure of the southern Chilean subduction zone (36 °S-42 °S) and its role in the gravity field. Geophysical Journal International 170, 995–1014. doi:10.1111/j.1365-246X.2007.03466.x.

Ulmer, P., Trommsdorff, V., 1995. Serpentine stability to mantle depths and subduction-related magmatism. Science 268, 858–861. doi:10.1126/science.268.5212.858.

Vlaar, N., Wortel, M., 1976. Lithospheric aging, instability and subduction. Tectonophysics 32, 331–351. doi:10.1016/0040-1951(76)90068-8.

Wada, I., Behn, M.D., Shaw, A.M., 2012. Effects of heterogeneous hydration in the incoming plate, slab rehydration, and mantle wedge hydration on slab-derived H2O flux in subduction zones. Earth and Planetary Science Letters 353-354, 60–71. doi:10.1016/j.epsl.2012.07.025.

Wayte, G.J., Worden, R.H., Rubie, D.C., Droop, G.T.R., 1989. A TEM study of disequilibrium plagioclase breakdown at high pressure: the role of infiltrating fluid. Contributions to Mineralogy and Petrology 101, 426–437. doi:10.1007/BF00372216.

Zhao, D., 2001. Seismic structure and origin of hotspots and mantle plumes. Earth and Planetary Science Letters 192, 251–265.